Journal of Colloid and Interface Science 660 (2024) 314–320

Contents lists available at ScienceDirect

Journal of Colloid And Interface Science

journal homepage: www.elsevier.com/locate/jcis

Regular Article

Dynamics of anisotropic colloidal systems: What to choose, DLS, DDM or XPCS?

Md. Arif Kamal [a,1], Matteo Brizioli [b], Thomas Zinn [c,2], Theyencheri Narayanan [c], Roberto Cerbino [d], Fabio Giavazzi [b], Antara Pal [e,f,*]

[a] Division of Physical Chemistry, Department of Chemistry, Lund University, Lund, Sweden
[b] Department of Medical Biotechnology and Translational Medicine, University of Milan, Milan, Italy
[c] ESRF-The European Synchrotron, Grenoble, France
[d] Faculty of Physics, University of Vienna, Vienna, Austria
[e] Department of Physics, Stockholm University, Stockholm, Sweden
[f] MAX IV Laboratory, Lund, Sweden

GRAPHICAL ABSTRACT

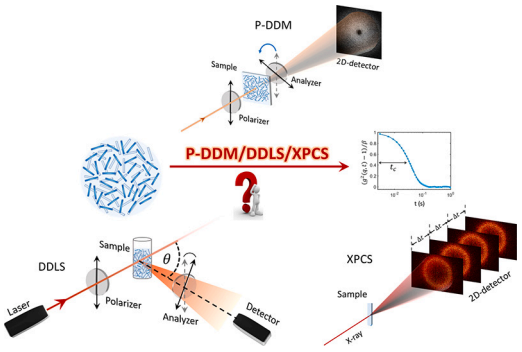

ABSTRACT

Investigation of the dynamics of colloids in bulk can be hindered by issues such as multiple scattering and sample opacity. These challenges are exacerbated when dealing with inorganic materials. In this study, we employed a model system of Akaganeite colloidal rods to assess three leading dynamics measurement techniques: 3D-(depolarized) dynamic light scattering (3D-(D)DLS), polarized-differential dynamic microscopy (P-DDM), and x-ray photon correlation spectroscopy (XPCS). Our analysis revealed that the translational and rotational diffusion coefficients captured by these methods show a remarkable alignment. Additionally, by examining the q-ranges and maximum volume fractions for each approach, we offer insights into the best technique for investigating the dynamics of anisotropic systems at the colloidal scale.

0. Introduction

Self-assembly is a ubiquitous process which is employed by nature to create hierarchical structures with designated functionalities.

* Corresponding author.
E-mail address: antara.pal@fkem1.lu.se (A. Pal).
[1] Current address: Department of Biomedical Science, Malmö University, Malmö, Sweden.
[2] Current address: Diamond Light Source Ltd., Didcot, UK.

https://doi.org/10.1016/j.jcis.2023.12.163
Received 16 October 2023; Received in revised form 11 December 2023; Accepted 28 December 2023
Available online 4 January 2024

Rather than confining itself to isotropic elements like spheres, nature also employs anisotropic components such as rods, cylinders, plates, and ellipsoids, among others. The shape of these building blocks not only affects the spatial arrangement of the self-assembled entities but also their translational and rotational dynamics.

Being the simplest model system, the dynamic behavior of spherical colloids has been extensively investigated. Existing literature reveals a good agreement between theory, simulations, and experiments for these isotropic systems [1–3]. Conversely, for anisotropic colloids, well established theory and predictions are mainly limited to dilute systems [4–9]. The theoretically predicted values of both the translational and rotational diffusion coefficients for these systems are in good agreement with experiments that have been performed primarily using dynamic light scattering (DLS) [10–19]. However, standard DLS technique is limited to systems with negligible contributions from multiple scattering. For larger particle sizes with high scattering contrast this immediately limits the technique to very low concentrations. Continuous developments in DLS techniques thus tried to overcome this limitation, thereby facilitating the measurement of the translational diffusion in semi-turbid samples exploiting advanced cross-correlation schemes, as in two-color DLS and in 3D-DLS [20–25]. In a very recent development, by implementing depolarized measurement in 3D-DLS mode, Pal et al. [26] have demonstrated the possibility to measure the rotational diffusion for semi-turbid anisotropic colloids.

Beyond conventional light scattering techniques, Differential Dynamic Microscopy (DDM) offers an alternative approach [27,28]. Compared to DLS, DDM allows to measure the translational diffusion from comparatively opaque colloidal dispersions [29–33]. Recent DDM-based studies have succeeded in measuring the roto-translational diffusion coefficients for (semi-) turbid systems [34–36]. In [34], using polarized-DDM Giavazzi et al. have successfully characterized the roto-translational diffusion of colloidal particles obtained by polymerizing an emulsion of droplets of liquid crystal in a nematic phase. Since the probing wavelength for both these techniques lies in the optical range, it is not completely possible to by-pass the issues related to opacity and multiple scattering at high concentrations, though in comparison DDM turns out to be a more suitable technique than DLS at high concentration.

Due to technological advancements, synchrotron-based multi-speckle X-ray Photon Correlation Spectroscopy (XPCS) has emerged as an alternative method for investigating dynamics at the colloidal length scale [37–46]. The fundamental principle of XPCS is akin to that of DLS, and the employment of coherent X-rays, as opposed to visible light, effectively addresses challenges such as multiple scattering and absorption commonly encountered in DLS and, to a lesser extent, in DDM when examining opaque or turbid systems, particularly those consisting of inorganic materials. It has been empirically demonstrated that XPCS can be utilized to explore the translational dynamics of anisotropic colloids composed of inorganic materials, not only at low concentrations but even well above the glass transition threshold owing to the smaller scattering cross-section [37,41,42,47–49].

In this article, we have investigated the dynamics of Akaganeite-based colloidal rods using three distinct techniques 3D-(D)DLS (3D-(depolarized) dynamic light scattering), P-DDM (polarized-DDM), and XPCS. We discuss advantages and limitations of each technique and identify the conditions under which one method outperforms the others in delivering comprehensive insights into the dynamics of anisotropic systems. We find that 3D-(D)DLS allows for the measurement of both the translational diffusion coefficient D_t and the rotational diffusion coefficient D_r up to a volume fraction $\phi = 3.1\times10^{-4}$, which is much below the formation of any structural correlation. With P-DDM, it is possible to measure at least up to $\phi = 1.25\times10^{-2}$, with potential for further extension as evidenced by previous studies on hematite ellipsoids extending measurements up to glass transition concentration [31]. With XPCS, D_t can be measured up to the formation of smectic phase at $\phi = 0.3$. Although XPCS holds the potential for incorporating polarization analysis

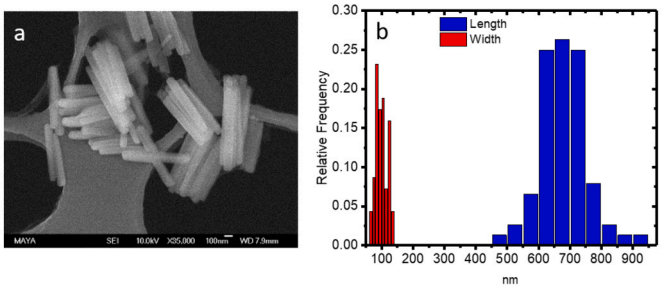

Fig. 1. (a) Representative SEM images for Akaganeite-based colloidal rods of aspect ratios $rho = 7.2$ and (b) represents the statistical distribution of length scales as has been obtained from (a).

to measure D_r, this is presently not done due to absorption losses and parasitic background. Using angular-temporal cross-correlation analysis, D_r may be obtained [50], but the accuracy of this method is not tested due to the computational complexity. At concentrations much below the formation of the structural correlation, a comparison of the D_t values obtained from all the three different techniques indicate that they are in good agreement with each other. Furthermore, similar values were also obtained for D_r from 3D-DDLS and P-DDM.

1. Experimental section

1.1. Synthesis

Reagent grade Ferric Chloride hexahydrate was purchased from Sigma-Aldrich and used without further purification. HCl obtained from VWR was used for all the experiments. Colloidal rods were synthesized according to the procedure described in [51]. Briefly, 1 ml of HCl (0.05M) was added to 4 ml of aqueous solution of FeCl3.6H2O (1M). 15 mL of Milli-Q water was added to the mixture to obtain a final volume of 20 mL. The solution was passed through 0.22 μm Millipore filters to remove any particulate contaminants and stored in a clean glass bottle with Teflon-lined screw cap. The glass bottle was tightly capped and placed in a preheated oven at 100 °C for 24 hrs. After aging, the samples were removed from the oven and quenched to room temperature under running tap water. The products were thoroughly cleaned using repeated cycles of centrifugation and dispersion in Milli-Q water.

1.2. Characterization and methods

1.2.1. Characterization using SEM

The characterization of the shape and size of the colloidal rods was carried out using Scanning electron microscopy (SEM) (ZEISS LEO Gemini 1560 and a ZEISS Gemini 500 at an accelerating voltage of 15 kV). From the resulting TEM images, using ImageJ, the particle size distribution was determined by analyzing at least 100 particles. Fig. 1(a) shows a representative micrograph of these rods while (b) represents the statistical size analysis based on these images. The particle long and short axes were found to be $a = 676 \pm 75$ nm and $b = 93.5 \pm 14$ nm, respectively, leading to an aspect ratio of $\rho = 7.2$.

1.2.2. 3D-(D)DLS

The DLS measurements were performed on a Mod3D-DLS Spectrometer (LS Instruments, Switzerland) that implements the modulated 3D cross correlation technology [25], equipped with 660 nm Cobolt laser with a maximum power of 100 mW. The apparatus is equipped with two Glan-Thompson polarizers at the detector side and two at the incident beam side. A VV geometry can be achieved by aligning the polarizers parallel to each other and VH geometry can be achieved by making them perpendicular to each other [26]. 5 mm cylindrical glass cells were used and placed in the temperature-controlled index matching

bath containing decalin. The scattered light was detected within a scattering angle range of 30 - 135° by avalanche photodiodes and processed by an LS Instrument correlator.

1.2.3. XPCS

Multispeckle ultrasmall-angle X-ray photon correlation spectroscopy (UA-XPCS) were performed at the beam line ID02, ESRF, in a pinhole ultrasmall-angle X-ray scattering (USAXS) geometry. This unique instrument allows XPCS measurements on particle suspensions down to the μm^{-1} q (wave vector) range [52]. The dispersions were filled in 0.5 mm glass capillaries. Experiments were performed using an X-ray of wavelength of 1.01 Å and a sample-to-detector distance of 30.55 m. The two dimensional speckle patterns were recorded using an EIGER 500K pixel array detector [52]. The correlation functions were calculated using the Dynamix software package, developed at the ESRF. The time and ensemble averaged intensity-intensity autocorrelation functions, $g^{(2)}(q,\Delta t)$, were obtained by the azimuthal averaging of pixel $g^{(2)}(q,\Delta t)$ corresponding to the same q using Dynamix package [53].

1.2.4. P-DDM

The suspensions of particles were filled in 200 μm thick rectangular glass capillaries and were imaged using a Nikon Eclipse Ti-E commercial microscope equipped with a camera (Hamamatsu Orca Flash 4.0 V2). We used a microscope objective with magnification M = 20X and numerical aperture NA = 0.4. The pixel size after magnification and 2×2 binning was equal to 0.645 μm. Unlike standard DDM, where no polarizing elements are used, the sample in this case was sandwiched between two polarizers. For this particular study, we have done two sets of measurements. For the first case, the polarizers were oriented parallel while for the second case, they were kept "almost crossed", at an angle 85° with respect to each other. A necessary condition for the validity of DDM analysis is the existence of a linear relationship between the intensity modulation in the image and the scattered field as discussed in detail in Ref. [35,54]. In (both polarized and non-polarized) bright-field microscopy this condition is fulfilled in the presence of a sufficiently strong transmitted *reference* wave which, acting as a local oscillator, enables heterodyne detection [54]. A non-zero angle between the polarizing elements is thus necessary to ensure the presence of the transmitted wave. The actual value of the angle between the polarizers can then be adjusted to tune the relative amplitude of the contributions from polarized (VV) and depolarized (VH) signals to the image structure function, respectively [35]. Two different acquisition schemes have been adopted according to the optical configuration (0° and 85° angle between the polarizers, respectively). In the first case, we collected two image sequences of $N = 10^4$ frames each, captured at frame rates $r = 400$ and $r = 50$ fps, respectively. In the second case, a single sequence of $N = 10^4$ frames at frame rate $r = 400$ was collected. As will be clear in the following, each acquisition protocol has been chosen to ensure adequate sampling over the whole interval of relaxation times accessible in the corresponding optical configuration. Each acquisition consists of a sequence of square images $I(\mathbf{x},t)$, where $\mathbf{x} = (x,y)$ indicates a position in the image plane (the z axis being oriented along the microscope optical axis) and the time variable t assumes only discrete values that are integer multiples of $1/r$. Each image was obtained with exposure time t_{exp} = 1.2 ms and has N_{pix} = 512 pixels per side. Once acquired and saved on disk, the image sequence was analyzed according to the usual DDM protocol. For each time delay $\Delta t = k/r$ of interest, where k is an integer, the difference signal $d(\mathbf{x},t_0,\Delta t) = [I(\mathbf{x},t_0+\Delta t) - I(\mathbf{x},t_0)]$ was calculated and its spatial Fourier power spectrum was computed by using a fast Fourier transform (FFT) routine. This procedure leads to the so-called *image structure function*

$$d_i(\mathbf{q},\Delta t) = \langle \left| FFT[d(\mathbf{x},t_0,\Delta t)] \right|^2 \rangle_{t_0} \tag{1}$$

that captures the dynamics of the sample as a function of the two-dimensional (2D) scattering wave-vector $\mathbf{q}$ and of the delay time Δt.

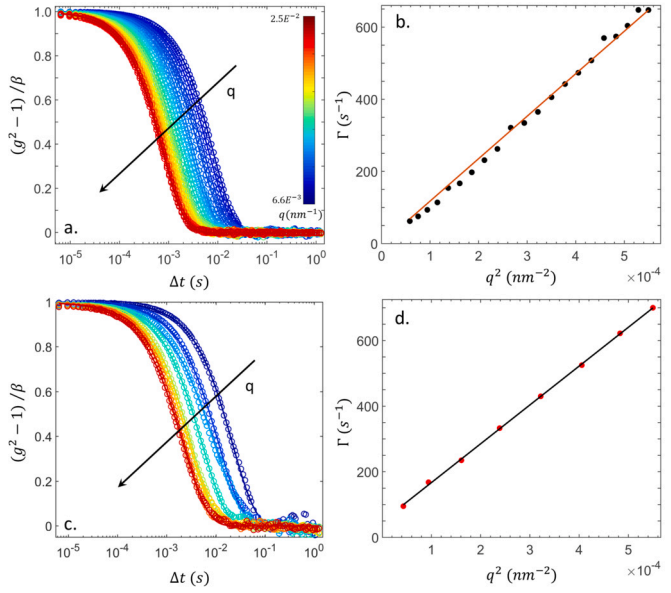

Fig. 2. (a) Intensity-intensity correlation functions for different q values as measured in VV geometry by 3D-DLS. (b) The experimentally obtained relaxation rate, Γ, as a function of q^2 as shown by the filled circles while the straight line shows the fit to it using $\Gamma = D_t q^2$. (c) Intensity autocorrelation functions for different q values as measured in VH geometry by 3D-DDLS. (d) The experimentally obtained relaxation rate, Γ, as a function of q^2 as shown by the filled circles while the straight line shows the fit to it using $\Gamma = D_t q^2 + 6D_r$. For (a) and (c) the open circles show the experimental observations and the continuous lines show the fit using eq. (5); different colors represent different q-values.

The image structure function is connected to the (normalized) image intermediate scattering function $f_i^{(1)}(\mathbf{q},\Delta t)$ [55] by the relation,

$$d_i(\mathbf{q},\Delta t) = 2A(\mathbf{q})[1 - f_i^{(1)}(\mathbf{q},\Delta t)] + 2B(\mathbf{q}) \tag{2}$$

where $B(\mathbf{q})$ is a term that accounts for the camera noise and $A(\mathbf{q})$ is an amplitude term that contains information about the static scattering from the sample and details about the imaging system [54]. For a collection of randomly oriented anisotropic particles, the image intermediate scattering function takes the form,

$$f_i^{(1)}(\mathbf{q},\Delta t) = \alpha(q) e^{-(\Gamma_1(q)\Delta t)^{\gamma_1}} + (1-\alpha(q))\, e^{-(\Gamma_2(q)\Delta t)^{\gamma_2}} \tag{3}$$

where $\Gamma_1(q) = D_t q^2$, and $\Gamma_2(q) = D_t q^2 + 6D_r$, D_t and D_r being the translational and rotational diffusion coefficients, respectively. γ_1 and γ_2 are the stretching parameters accounting for the polydispersity in the particle-size distribution. For free diffusion of a monodisperse system, the value of γ_1 and γ_2 should be 1. The weight $\alpha(q)$ depends on the relative amplitude of the polarized and the depolarized contribution to the intermediate scattering function [54].

All the DLS, DDM and XPCS measurements are done at room temperature.

1.3. Results and discussion

Both DLS and XPCS measurements allow one to obtain the information about the particle dynamics on a length scale, which is of the order of $1/q$ via the intensity-intensity auto-correlation function,

$$g^{(2)}(\mathbf{q},\Delta t) = \frac{\langle I(\mathbf{q},t) I(\mathbf{q},t+\Delta t)\rangle}{\langle I(\mathbf{q})\rangle^2} \tag{4}$$

where $\mathbf{q}$ is the scattering vector with magnitude, $q = 4\pi sin(\theta/2)/\lambda$, θ being the scattering angle and λ being the wavelength in the scattering medium.

Fig. 2 indicates the intensity-intensity correlation functions for different q as well as the relaxation rates (Γ) as a function of q^2 for

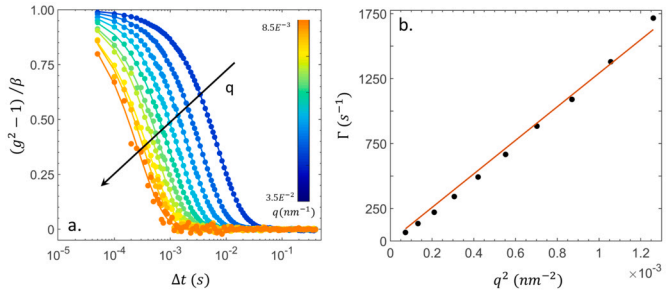

Fig. 3. (a) Intensity-intensity auto correlation functions for different q values as measured by XPCS. The filled circles show the experimental observations and the continuous lines show the fit using eq. (5); different colors represent different q-values. (b) The experimentally obtained relaxation rate, Γ, as a function of q^2 as shown by the filled circles while the straight line shows the fit to it using $\Gamma = D_t q^2$.

$\phi = 4.6 \times 10^{-5}$ as measured by 3D-(D)DLS. The upper panel shows the data in VV mode whereas the lower panel shows the data in VH mode. The intermediate scattering function $g^{(1)}(\mathbf{q}, \Delta t)$ is related to $g^{(2)}(\mathbf{q}, \Delta t)$ via Siegert relation, $g^{(1)}(\mathbf{q}, \Delta t) = \sqrt{[g^{(2)}(\mathbf{q}, \Delta t) - 1]/\beta}$, where β is a setup-dependent experimental parameter known as the contrast or coherence factor. $g^{(1)}(q, \Delta t)$ can be described phenomenologically by a single exponential function,

$$g^{(1)}(q, \Delta t) = \exp[-(\Gamma \Delta t)^{\gamma}] \tag{5}$$

where Γ is the relaxation rate of the particle diffusion and γ is the stretching parameter. For free diffusion of mono-disperse system, the value of γ should be 1.

Eq. (5) was used to analyze the data obtained from the 3D-DLS measurements (VV) (as shown in Fig. 2(a)) and Γ were extracted accordingly. The q-dependence of Γ is given by $\Gamma = D_t q^2$. Therefore, the translational diffusion coefficient D_t of the particles can be obtained from the angular dependence of Γ, as it is directly related to the slope of the data plotted as Γ vs q^2, as shown in Fig. 2(b). The value of D_t is found to be $1.20 \pm 0.02 \times 10^6 nm^2/s$.

The measured correlation functions obtained in the VH geometry are shown in Fig. 2(c). They are also well-described by Eq. (5), which we use to extract Γ, whose scaling with q is expected to be $\Gamma_1(q) = D_t q^2 + 6D_r$. In Fig. 2(d), we plot the experimentally determined Γ as a function of q^2 for the VH geometry. From the intercept of this we extract $D_r = 8.06 \pm 0.3/s$. As expected, the slopes of the Γ vs q^2 curves for the VV and the VH geometry are the same and for both we also find $\gamma = 1 \pm 0.02$.

Fig. 3 shows the data obtained with XPCS at $\phi = 0.0028$. A fitting to the correlation function was obtained using eq. (5) (Fig. 3(a)). The plot of Γ as a function of q^2, is shown in Fig. 3(b). In this case also the value of γ is found to be 1 ± 0.02. Further, from the slope of the curve we have calculated D_t, which is found to be $D_t = 1.29 \pm 0.05 \times 10^6 nm^2/s$. The values obtained from the DLS and XPCS measurement thus are in good agreement with each other, although the sample concentration measured by XPCS is 70 times higher than that measured by 3D-DLS. This is because in both cases the sample concentration is below the typical value at which the structural correlation starts to build up. As a result, for both these measurements, we are measuring the diffusion coefficient of free particles.

It is worthwhile to note that by using 3D-DLS we could measure only up to $\phi = 3.1 \times 10^{-4}$, whereas with XPCS it was possible to measure up to $\phi = 0.3$ (data is not shown here). Since we are measuring XPCS at a very large sample to detector distance of 30.55 m, the q-range almost overlaps with DLS. However, the current limitation with the XPCS technique is that the extraction of D_r is not straightforward.

Fig. 4 shows the data for the DDM measurement at $\phi = 4 \times 10^{-4}$. One can already observe two relaxation processes in the correlation functions (Fig. 4(a)), which have been measured by aligning the polarizers parallel to each other. Eq. (3) was used to fit the data. However, in this case, we have kept the value of γ_1 fixed at 1. Fig. 4(b) shows the variation of Γ_1 as a function of q^2. Similar to the previous cases, we have fit this with $\Gamma_1 = D_t q^2$ to get the value of D_t. The value of D_t is found to be $D_t = 1.27 \pm 0.06 \times 10^6 nm^2/s$ which also matches with our previous measurements with DLS and XPCS. Fig. 4(c) shows the variation of Γ_2 as a function of q^2. Similar to DLS measurement in VH geometry, we have fitted our data with $\Gamma = D_t q^2 + 6D_r$. The fitting procedure provides the estimates $D_r = 9.3 \pm 0.3/s$ and $D_t = 1.3 \pm 0.7 \times 10^6 nm^2/s$ for the rotational and the translational diffusion coefficients, respectively. The value of D_r obtained from the fit is in good agreement with DLS measurements. The estimated D_t, although affected by a large uncertainty, is fully compatible with the value extracted from the Γ_1 and with the ones obtained from both DLS and XPCS. Fig. 4(d) shows the correlation functions, which have been measured by orienting the polarizers at an angle 85° with respect to each other. In this case, the intermediate scattering function is dominated by the depolarized contribution, and one observes a single relaxation mode, which can be thus fitted with a simplified version of eq. (3), $f_i^{(1)}(\mathbf{q}, \Delta t) = e^{-(\Gamma(q)\Delta t)^{\gamma}}$, to obtain Γ. Fig. 4(e) represents the variation of Γ as a function of q^2, which has been fitted with $\Gamma = D_t q^2 + 6D_r$ to get D_t and D_r, which is found to be $D_t = 1.54 \pm 0.1 \times 10^6 nm^2/s$ and $D_r = 9.5 \pm 0.07/s$.

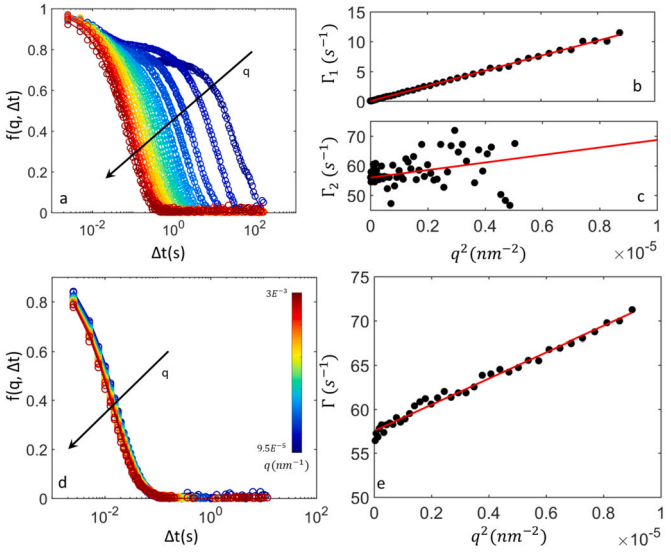

Fig. 4. (a) Normalized image structure functions for different q values as measured by P-DDM while keeping the polarizers parallel to each other. The open circles show the experimental observations and the continuous lines show the fit using eq. (3). (b) and (c) The experimentally obtained relaxation rates, Γ_1 and Γ_2, as a function of q^2 as shown by the filled circles while the continuous lines show the fit using $\Gamma = D_t q^2$ and $\Gamma = D_t q^2 + 6D_r$ respectively. (d) Normalized image structure functions for different q values as measured by P-DDM keeping the polarizers axes at an angle 85° with respect to each other. The open circles show the experimental observations and the continuous lines show the fit using eq. (3). (e) The experimentally obtained relaxation rates, Γ, as a function of q^2 as shown by the filled circles while the continuous lines show the fit using $\Gamma = D_t q^2 + 6D_r$. For (a) and (d) the open circles show the experimental observations and the continuous lines show the fit (blue being the smallest and red being the highest ones). (For interpretation of the colors in the figure(s), the reader is referred to the web version of this article.)

Although the measured D_t and D_r values are in good agreement with each other, one of the major differences between DLS, XPCS and DDM measurements lies in the accessible q-ranges. In a standard setup, as exemplified in this study, the accessible q-range for DDM spans from $10^{-4} nm^{-1} < q < 3 \times 10^{-3} nm^{-1}$. In contrast, for DLS the q-range is confined between $3.4 \times 10^{-3} nm^{-1} \leq q \leq 2.5 \times 10^{-2} nm^{-1}$ whereas XPCS in the USAXS range can cover $2 \times 10^{-3} nm^{-1} < q < 10^{-1} nm^{-1}$. Technically

Table 1
Summary of the different techniques, 3D-(D)DLS, XPCS and P-DDM.

Technique	Maximum ϕ	q range (nm^{-1})	D_t (nm^2/s)	D_r (s^{-1})
3D-(D)DLS	3.1×10^{-4}	$3.4\times10^{-3}\le q\le 2.5\times10^{-2}$	$1.2\pm0.02\times10^{6}$	8.06 ± 0.3
XPCS (USAXS range)	0.3	$2\times10^{-3}<q<10^{-1}$	$1.29\pm0.05\times10^{6}$	—
P-DDM	1.25×10^{-2}	$10^{-4}<q<3\times10^{-3}$	$1.27\pm0.06\times10^{6}$	9.3 ± 0.3
calculated following Ref. [56,57]	—	—	$1.5\pm0.2\times10^{6}$	19 ± 6
calculated following Ref. [58]	—	—	$1.2\pm0.1\times10^{6}$	17 ± 6

XPCS can cover the q-range lying between $10^{-3}nm^{-1}\le q\le 3\times10nm^{-1}$. However, for XPCS, the main limitation is from the scattering power of the sample. If the dynamics is very fast, there are not enough photons scattered to construct a correlation function with short lag times. As a result, the higher q range is essentially limited by the magnitude of the relaxation rate.

For P-DDM measurement, when we have kept the polarizer and analyzer parallel to each other, two decay processes are visible in $f(q,\Delta t)$. However, this is not the case for DLS measurement in VV geometry. It is important to point out that in general the field cross correlation function $g^{(1)}_{vv}$, is not characterized by a single exponential decay for optically anisotropic particles. In this case, since the q-range is much higher for DLS than DDM we do not observe them for DLS but for DDM.

2. Conclusion

In this study, we have undertaken a comparative analysis of three advanced measurement techniques-3D-(D)DLS, P-DDM, and XPCS-utilized for probing dynamics at the colloidal length scale as shown in Table 1. The translational diffusion coefficients (D_t) derived from these methods are in strong agreement. Rotational diffusion (D_r) can be assessed using either 3D-DDLS or P-DDM, and the values obtained are consistent with each other; however, measurement of D_r with XPCS is not well-established at the moment. With the development of the fourth generation synchrotron sources, we hope that the depolarized-XPCS measurement will become possible or the angular cross-correlation analysis will be more established in near future. The accessible wave vector ranges for DLS and XPCS (when operated in ultra-small angle mode) align closely, whereas DDM enables access to even smaller q-ranges.

It is instructive to compare our experimental findings with the values of the translational and rotational diffusion coefficients obtained by combining the geometric information from EM with two commonly used theoretical models by Tirado and Garcia de la Torre [56,57] and Broersma [58], respectively. We obtain $D_t = 1.5\pm0.2\times10^{6}nm^2/s$, $D_r = 19\pm6/s$ (Tirado and Garcia de la Torre), and $D_t = 1.2\pm0.1\times10^{6}nm^2/s$, $D_r = 17\pm6/s$ (Broersma). We note that, while the values for the translational diffusion coefficient are fully compatible with our experimental estimate $D_t = 1.3\pm0.1\times10^{6}nm^2/s$, the predicted rotational diffusion coefficients are significantly larger (by about a factor of two) then the experimental one $D_r = 9\pm1/s$. Currently, we do not have a clear explanation of this deviation. We note however, that similar discrepancies between predicted and measured rotational diffusion coefficients are consistently reported in the literature (see e.g. Ref. [10]) and often attributed to a combination of non-ideality of the particle shape, uncontrolled absorption of molecules (like surfactants) on the particle surface and increased friction due to electrostatic effects.

Our experiments employed colloidal dispersions in a dilute regime – a situation where no interparticle interactions are present. As a result, structural correlations are absent between particles. The colloidal particles used in our experiments are made up of inorganic material which renders them opaque. We find that in the case of DLS it is not possible to measure at concentrations where structural correlation starts to build up. Comparatively, DDM turns out to be a better technique as it allows for the measurement of the dynamics at higher sample concentrations. However, DDM reaches its limitation when the sample concentration becomes so high that the particles start to self-assemble into higher order structures (like liquid crystalline phases for colloidal rods). For our experiments we have used the standard sample cells for all the three techniques. As a result, one needs to pay a particular attention to the fact that the path length for DLS, DDM and XPCS are not the same. One can push the limit of opacity within a range by playing with the thickness of the samples. So the take home message is that one should choose the measurement techniques not only depending on the length scale (which means accessible q-ranges) but also carefully considering the opacity of the samples. The strength of XPCS is for probing higher volume fractions and slower dynamics, while DLS is superior for extremely dilute samples. Moreover, XPCS requires access to a specialized instrument at a large scale facility.

Our experiments employed colloidal dispersions in a dilute regime – a situation where no interparticle interactions are present. As a result, structural correlations are absent between particles. The colloidal particles used in our experiments are made up of inorganic material which renders them opaque. We find that in the case of DLS it is not possible to measure at concentrations where structural correlation starts to build up. Comparatively, DDM turns out to be a better technique as it allows for the measurement of the dynamics at higher sample concentrations. However, DDM reaches its limitation when the sample concentration becomes so high that the particles start to self-assemble into higher order structures (like liquid crystalline phases for colloidal rods). For our experiments we have used the standard sample cells for all the three techniques. As a result, one needs to pay a particular attention to the fact that the path length for DLS, DDM and XPCS are not the same. One can push the limit of opacity within a range by playing with the thickness of the samples. So the take home message is that one should choose the measurement techniques not only depending on the length scale (which means accessible q-ranges) but also carefully considering the opacity of the samples. The strength of XPCS is for probing higher volume fractions and slower dynamics, while DLS is superior for extremely dilute samples. Moreover, XPCS requires access to a specialized instrument at a large scale facility.

The nature of the detector is another important aspect that should be taken into consideration. For DDM and XPCS, we have used 2D detectors in our experiments. The 2D nature of the intermediate scattering function provides in general a powerful way to study the dynamics along different directions in the **q** plane that might be of particular interest for the problem under study [59]. In addition, the ensemble averaged $g^{(2)}(q,\Delta t)$ can also be readily obtained with the use of a 2D detector.

CRediT authorship contribution statement

Md. Arif Kamal: Formal analysis, Investigation, Writing – original draft, Writing – review & editing. **Matteo Brizioli:** Formal analysis, Investigation. **Thomas Zinn:** Investigation, Writing – review & editing. **Theyencheri Narayanan:** Investigation, Writing – review & editing. **Roberto Cerbino:** Writing – review & editing. **Fabio Giavazzi:** Formal analysis, Investigation, Writing – review & editing. **Antara Pal:** Conceptualization, Formal analysis, Investigation, Project administration, Writing – original draft, Writing – review & editing.

Declaration of competing interest

The authors declare that they have no known competing financial interests or personal relationships that could have appeared to influence the work reported in this paper.

Data availability

Data will be made available on request.

Acknowledgements

Peter Schurtenberger is acknowledged for providing support, Daniel Madsen is acknowledged for helping with the SEM measurement. Peter Holmqvist is acknowledged for many helpful discussions. Financial support from the Röntgen-Ångström Cluster Grant No. 2019-06075, and European Union's Horizon 2020 research and innovation program through the European Soft Matter Infrastructure grant (731019-EUSMI) are gratefully acknowledged. ESRF is acknowledged for granting beam time (SC-5054).

References

[1] S. Golde, T. Palberg, H.J. Schöpe, Correlation between dynamical and structural heterogeneities in colloidal hard-sphere suspensions, Nat. Phys. 12 (2016) 712.
[2] A.J. Banchio, M. Heinen, P. Holmqvist, G. Nägele, Short- and long-time diffusion and dynamic scaling in suspensions of charged colloidal particles, J. Chem. Phys. 148 (2018).
[3] F. Westermeier, B. Fischer, W. Roseker, G. Grübel, G. Nägele, M. Heinen, Structure and short-time dynamics in concentrated suspensions of charged colloids, J. Chem. Phys. 137 (2012).
[4] J.K. Dhont, An Introduction to Dynamics of Colloids, Elsevier, 1996.
[5] J. Elgeti, R.G. Winkler, G. Gompper, Physics of microswimmer single particle motion and collective behavior: a review, Rep. Prog. Phys. 78 (2015) 056601.
[6] S. Jabbari-Farouji, E. Trizac, Dynamic Monte Carlo simulations of anisotropic colloids, J. Chem. Phys. 137 (2012).
[7] M. Rex, H. Wensink, H. Löwen, Dynamical density functional theory for anisotropic colloidal particles, Phys. Rev. E 76 (2007) 021403.
[8] A. Ortega, J. Garcıa de la Torre, Hydrodynamic properties of rodlike and disklike particles in dilute solution, J. Chem. Phys. 119 (2003) 9914.
[9] F. Perrin, Mouvement brownien d'un ellipsoide (ii). Rotation libre et dépolarisation des fluorescences. Translation et diffusion de molécules ellipsoidales, J. Phys. Radium 7 (1936) 1.
[10] A. Günther, P. Bender, A. Tschöpe, R. Birringer, Rotational diffusion of magnetic nickel nanorods in colloidal dispersions, J. Phys. Condens. Matter 23 (2011) 325103.
[11] D. Kleshchanok, M. Heinen, G. Nägele, P. Holmqvist, Dynamics of charged gibbsite platelets in the isotropic phase, Soft Matter 8 (2012) 1584.
[12] I. Martchenko, H. Dietsch, C. Moitzi, P. Schurtenberger, Hydrodynamic properties of magnetic nanoparticles with tunable shape anisotropy: prediction and experimental verification, J. Phys. Chem. B 115 (2011) 14838.
[13] R. Nixon-Luke, G. Bryant, A depolarized dynamic light scattering method to calculate translational and rotational diffusion coefficients of nanorods, Part. Part. Syst. Charact. 36 (2019) 1800388.
[14] J. Rodríguez-Fernández, J. Pérez-Juste, L.M. Liz-Marzán, P.R. Lang, Dynamic light scattering of short au rods with low aspect ratios, J. Phys. Chem. C 111 (2007) 5020.
[15] D. Feller, M. Otten, M. Hildebrandt, M. Krüsmann, G. Bryant, M. Karg, Translational and rotational diffusion coefficients of gold nanorods functionalized with a high molecular weight, thermoresponsive ligand: a depolarized dynamic light scattering study, Soft Matter 17 (2021) 4019.
[16] D. Lehner, H. Lindner, O. Glatter, Determination of the translational and rotational diffusion coefficients of rodlike particles using depolarized dynamic light scattering, Langmuir 16 (2000) 1689.
[17] B.M. van der Zande, J.K. Dhont, M.R. Böhmer, A.P. Philipse, Colloidal dispersions of gold rods characterized by dynamic light scattering and electrophoresis, Langmuir 16 (2000) 459.
[18] A.M. Shetty, G.M. Wilkins, J. Nanda, M.J. Solomon, Multiangle depolarized dynamic light scattering of short functionalized single-walled carbon nanotubes, J. Phys. Chem. C 113 (2009) 7129.
[19] S. Jabbari-Farouji, E. Eiser, G.H. Wegdam, D. Bonn, Ageing dynamics of translational and rotational diffusion in a colloidal glass, J. Phys. Condens. Matter 16 (2004) L471.
[20] M. Medebach, C. Moitzi, N. Freiberger, O. Glatter, Dynamic light scattering in turbid colloidal dispersions: a comparison between the modified flat-cell light-scattering instrument and 3d dynamic light-scattering instrument, J. Colloid Interface Sci. 305 (2007) 88.
[21] E. Overbeck, C. Sinn, T. Palberg, K. Schätzel, Probing dynamics of dense suspensions: three-dimensional cross-correlation technique, Colloids Surf. A, Physicochem. Eng. Asp. 122 (1997) 83.
[22] P. Pusey, Suppression of multiple scattering by photon cross-correlation techniques, Curr. Opin. Colloid Interface Sci. 4 (1999) 177.
[23] K. Schätzel, Suppression of multiple scattering by photon cross-correlation techniques, J. Mod. Opt. 38 (1991) 1849.
[24] C. Urban, P. Schurtenberger, Characterization of turbid colloidal suspensions using light scattering techniques combined with cross-correlation methods, J. Colloid Interface Sci. 207 (1998) 150.
[25] I.D. Block, F. Scheffold, Modulated 3d cross-correlation light scattering: improving turbid sample characterization, Rev. Sci. Instrum. 81 (2010).
[26] A. Pal, P. Holmqvist, A. Vaccaro, P. Schurtenberger, Extending depolarized dls measurements to turbid samples, J. Colloid Interface Sci. 627 (2022) 1.
[27] R. Cerbino, V. Trappe, Differential dynamic microscopy: probing wave vector dependent dynamics with a microscope, Phys. Rev. Lett. 100 (2008) 188102.
[28] F. Giavazzi, R. Cerbino, Digital Fourier microscopy for soft matter dynamics, J. Opt. 16 (2014) 083001.
[29] F. Giavazzi, G. Savorana, A. Vailati, R. Cerbino, Structure and dynamics of concentration fluctuations in a non-equilibrium dense colloidal suspension, Soft Matter 12 (2016) 6588.
[30] R. Nixon-Luke, J. Arlt, W.C. Poon, G. Bryant, V.A. Martinez, Probing the dynamics of turbid colloidal suspensions using differential dynamic microscopy, Soft Matter 18 (2022) 1858.
[31] A. Pal, V.A. Martinez, T.H. Ito, J. Arlt, J.J. Crassous, W.C. Poon, P. Schurtenberger, Anisotropic dynamics and kinetic arrest of dense colloidal ellipsoids in the presence of an external field studied by differential dynamic microscopy, Sci. Adv. 6 (2020) eaaw9733.
[32] M. Reufer, V.A. Martinez, P. Schurtenberger, W.C. Poon, Differential dynamic microscopy for anisotropic colloidal dynamics, Langmuir 28 (2012) 4618.
[33] R. Nixon-Luke, G. Bryant, Differential dynamic microscopy to measure the translational diffusion coefficient of nanorods, J. Phys. Condens. Matter 32 (2019) 115102.
[34] F. Giavazzi, A. Pal, R. Cerbino, Probing roto-translational diffusion of small anisotropic colloidal particles with a bright-field microscope, Eur. Phys. J. E 44 (2021) 61.
[35] F. Giavazzi, C. Haro-Pérez, R. Cerbino, Simultaneous characterization of rotational and translational diffusion of optically anisotropic particles by optical microscopy, J. Phys. Condens. Matter 28 (2016) 195201.
[36] R. Cerbino, D. Piotti, M. Buscaglia, F. Giavazzi, Dark field differential dynamic microscopy enables accurate characterization of the roto-translational dynamics of bacteria and colloidal clusters, J. Phys. Condens. Matter 30 (2017) 025901.
[37] A. Pal, T. Zinn, M.A. Kamal, T. Narayanan, P. Schurtenberger, Anomalous dynamics of magnetic anisotropic colloids studied by xpcs, Small 14 (2018) 1802233.
[38] A. Pal, M.A. Kamal, T. Zinn, J.K. Dhont, P. Schurtenberger, Anisotropic dynamics of magnetic colloidal cubes studied by X-ray photon correlation spectroscopy, Phys. Rev. Mater. 5 (2021) 035603.
[39] A.J. Banchio, J. Gapinski, A. Patkowski, W. Häußler, A. Fluerasu, S. Sacanna, P. Holmqvist, G. Meier, M.P. Lettinga, G. Nägele, Many-body hydrodynamic interactions in charge-stabilized suspensions, Phys. Rev. Lett. 96 (2006) 138303.
[40] A. Robert, E. Wandersman, E. Dubois, V. Dupuis, R. Perzynski, Glassy dynamics and aging in a dense ferrofluid, Europhys. Lett. 75 (2006) 764.
[41] A. Pal, M.A. Kamal, P. Schurtenberger, Structure and anisotropic dynamics of stimuli responsive colloidal ellipsoids at the nearest neighbor length scale, J. Colloid Interface Sci. 621 (2022) 352.
[42] A. Pal, M.A. Kamal, P. Holmqvist, P. Schurtenberger, Structure and dynamics of dense colloidal ellipsoids at the nearest-neighbor length scale, Phys. Rev. Res. 3 (2021) 023254.
[43] T. Zinn, L. Sharpnack, T. Narayanan, Dynamics of magnetic Janus colloids studied by ultra small-angle X-ray photon correlation spectroscopy, Soft Matter 19 (2023) 2311.
[44] T. Hoshino, M. Nakayama, Y. Hosokawa, K. Mochizuki, S. Kajiyama, Y. Kohmura, T. Kato, Experimental probing of dynamic self-organized columnar assemblies in colloidal liquid crystals, Nanoscale Adv. (2023).
[45] Y. Chushkin, A. Gulotta, F. Roosen-Runge, A. Pal, A. Stradner, P. Schurtenberger, Probing cage relaxation in concentrated protein solutions by X-ray photon correlation spectroscopy, Phys. Rev. Lett. 129 (2022) 238001.
[46] J. Wagner, C. Märkert, B. Fischer, L. Müller, Direction dependent diffusion of aligned magnetic rods by means of X-ray photon correlation spectroscopy, Phys. Rev. Lett. 110 (2013) 048301.
[47] A. Schavkan, Dynamics of colloidal systems of magnetic nanoparticles under influence of magnetic fields investigated by XPCS, Ph.D. thesis, Staats-und Universitätsbibliothek Hamburg Carl von Ossietzky, 2017.
[48] T. Hoshino, M. Nakayama, S. Fujinami, T. Nakatani, Y. Kohmura, T. Kato, Static structure and dynamical behavior of colloidal liquid crystals consisting of hydroxyapatite-based nanorod hybrids, Soft Matter 15 (2019) 3315.
[49] P. Holmqvist, V. Meester, F. Westermeier, D. Kleshchanok, Rotational diffusion in concentrated platelet systems measured with X-ray photon correlation spectroscopy, J. Chem. Phys. 139 (2013).
[50] Z. Hu, J.J. Donatelli, J.A. Sethian, Cross-correlation analysis of X-ray photon correlation spectroscopy to extract rotational diffusion coefficients, Proc. Natl. Acad. Sci. 118 (2021) e2105826118.

[51] E. Matijević, P. Scheiner, Ferric hydrous oxide sols: III. Preparation of uniform particles by hydrolysis of fe (iii)-chloride, -nitrate, and -perchlorate solutions, J. Colloid Interface Sci. 63 (1978) 509.
[52] T. Zinn, A. Homs, L. Sharpnack, G. Tinti, E. Fröjdh, P.-A. Douissard, M. Kocsis, J. Möller, Y. Chushkin, T. Narayanan, Ultra-small-angle X-ray photon correlation spectroscopy using the Eiger detector, J. Synchrotron Radiat. 25 (2018) 1753.
[53] P. Paleo, J. Kieffer, Y. Chushkin, Dynamix v0.2: XPCS data reduction python (v0.2), https://doi.org/10.5281/zenodo.5520626, 2021.
[54] F. Giavazzi, D. Brogioli, V. Trappe, T. Bellini, R. Cerbino, Scattering information obtained by optical microscopy: differential dynamic microscopy and beyond, Phys. Rev. E 80 (2009) 031403.
[55] R. Pecora, Dynamic Light Scattering: with Applications to Chemistry, Biology, and Physics, Dover Publications, 2000.
[56] M.M. Tirado, J.G. de la Torre, Translational friction coefficients of rigid, symmetric top macromolecules. Application to circular cylinders, J. Chem. Phys. 71 (1979) 2581.
[57] M.M. Tirado, J.G. De La Torre, Rotational dynamics of rigid, symmetric top macromolecules. Application to circular cylinders, J. Chem. Phys. 73 (1980) 1986.
[58] J. Newman, H.L. Swinney, L.A. Day, Hydrodynamic properties and structure of fd virus, J. Mol. Biol. 116 (1977) 593.
[59] F. Giavazzi, S. Crotti, A. Speciale, F. Serra, G. Zanchetta, V. Trappe, M. Buscaglia, T. Bellini, R. Cerbino, Viscoelasticity of nematic liquid crystals at a glance, Soft Matter 10 (2014) 3938.